Physical Science International Journal

26(6): 17-28, 2022; Article no.PSIJ.93484
ISSN: 2348-0130

Proposal and Simulation of a Doubly Fed Induction Generator for the Coastal Zone of Benin

D'Almeida Renaud Philippe [a*], Agbokpanzo Richard G. [b] and Agbomahena Macaire [a]

[a] EPAC/UAC, Abomey-Calavi, Benin.
[b] ENSET/UNSTIM, Lokossa, Benin.

Authors' contributions

This work was carried out in collaboration among all authors. All authors read and approved the final manuscript.

Article Information

DOI: 10.9734/PSIJ/2022/v26i6748

Open Peer Review History:
This journal follows the Advanced Open Peer Review policy. Identity of the Reviewers, Editor(s) and additional Reviewers, peer review comments, different versions of the manuscript, comments of the editors, etc are available here: https://www.sdiarticle5.com/review-history/93484

Original Research Article

Received 05 September 2022
Accepted 07 November 2022
Published 09 November 2022

ABSTRACT

This paper presents the sizing of a Doubly Fed Induction Generator (DFIG) with a power of 690.747 kW for the coastal area of Benin. The sizing of the proposed DFIG starts from the power density of the offshore wind potential of Benin obtained at 80 m at the sea surface to determine the power of the generator. Thanks to the geometrical, electrical and magnetic parameters obtained after sizing, the simulation of the generator operation was done using the finite element analysis (FEA). This simulation is done by running the generator at nominal speed in supersynchronous mode. The results of this simulation show that the powers obtained are close to the expected theoretical values. The curves of the powers and those of the flux densities in the air gap of the generator are presented. Electromagnetic model results are then used to develop the thermal model of the generator. The results of the thermal analysis obtained after simulation by the FEA allowed us to know the temperature values in each region of the DFIG.

Keywords: DFIG; FEA; power density; electromagnetic model; thermal model.

1. INTRODUCTION

The request for electrical energy in Benin is becoming more and more important every year and the coverage of the country in energy still remains a major problem today. One of the measures of the Beninese government's action program is to develop renewable energies to improve the living conditions of the population by reducing their difficulties in accessing electrical energy [1,2].

**Corresponding author: E-mail: renaudjdd@yahoo.fr, renaudjdd@gmail.com;*

Several projects for the production of electrical energy from renewable sources are therefore underway. But most of these projects are based on solar energy. However, studies conducted in [3] have shown that Benin has a good offshore wind energy potential. In addition to the available solar energy, Benin must exploit its offshore wind potential to better strengthen its energy mix. The choice of the generator adapted to the production of electrical energy by wind turbine in an offshore environment requires to be made by taking into account the various parameters related to the environment, to the structure of the generator, to its operation in nominal regime, to its heating, etc. In this context, this paper proposed the sizing of a DFIG for the generation of electric energy by wind turbine. The goal is to produce a technical document exploitable by the manufacturers for the design of the DFIG adapted to the offshore wind profile of Benin. In this paper, the power of the generator is first determined from the power density. Knowing this power, the sizing technique to find the geometrical parameters of the DFIG is developed. The geometrical and electrical parameters found were then used to build the dynamic model by FEA under flux-2D, 2022 version software. From this model the powers developed in the stator, in the rotor as well as the total power for an operation in nominal regime are obtained. theses powers are close to the calculated theoretical powers. Then the thermal model of the DFIG is developed by determining the steady state temperature distribution in the active parts by FEA. The results obtained are satisfactory and can be used for the design of the DFIG. In addition, to complete this work, a study on the optimization and control of the DFIG is underway.

This paper is subdivided into three main parts. In the first part the operation of the DFIG in a wind power system is described. The second part shows the sizing and simulation steps of the DFIG for the chosen area. Finally, In the third part, the thermal model of the sized DFIG is presented.

2. DESCRIPTION OF THE OPERATION OF THE DFIG IN A WIND POWER SYSTEM

The wind turbine power generation system (Fig. 1) generally consists of a turbine that rotates using the kinetic energy of the wind. This turbine is usually coupled to a generator through a gearbox. The generator transforms the mechanical energy received by the turbine into electrical energy. The step-up transformer allows the connection to the distribution grid.

DFIG is the most commonly used generator in wind energy, especially in offshore environments, as it offers great operating advantages. This generator is connected on the stator side directly to the electrical grid while its rotor is connected to the grid via a converter. This latter includes an intermediate DC bus and two reversible AC-DC stages. The DFIG operates at a variable speed of about ±30% of the synchronous speed (Ω_s). It can operate in subsynchronous mode where the rotational speed (Ω) is lower than the synchronous speed ($\Omega < \Omega_s$) or in supersynchronous mode where the rotational speed is higher than the synchronous speed ($\Omega > \Omega_s$) [4–6].

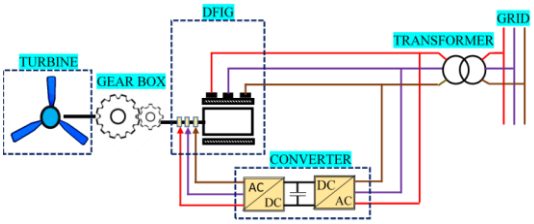

Fig. 1. Wind turbine power generation system

3. DFIG SIZING AND SIMULATION

In this part the sizing flowchart of the DFIG is shown in Fig. 2.

To determine the power of the generator, a zone located at sea at 10 km from the Beninese coast is chosen. The coordinates of this zone are 6.25°N in North latitude and 2.25°E in East longitude (Fig. 3).

A horizontal axis wind turbine located at a height of 80m from the sea surface is chosen. The curves of the distribution of the power density available at 80m in the exclusive economic zone of Benin are plotted and presented in [3].

It is important to notice that the potential varies between $612\,W/m^2$ and $850.4\,W/m^2$ .This is excellent for the production of offshore wind energy. By exploiting these curves, the power density (D_p) for the coordinates of the chosen area is deducted. Then it can be seen that $D_p = 799.5336\,W/m^2$ for this zone. The available wind power (P_w) is given by the following equation (1) [8]:

$$P_w = D_p.\pi R^2 \qquad (1)$$

Where P_w is the wind power, D_p the power density and R the radius of the turbine in m/s.

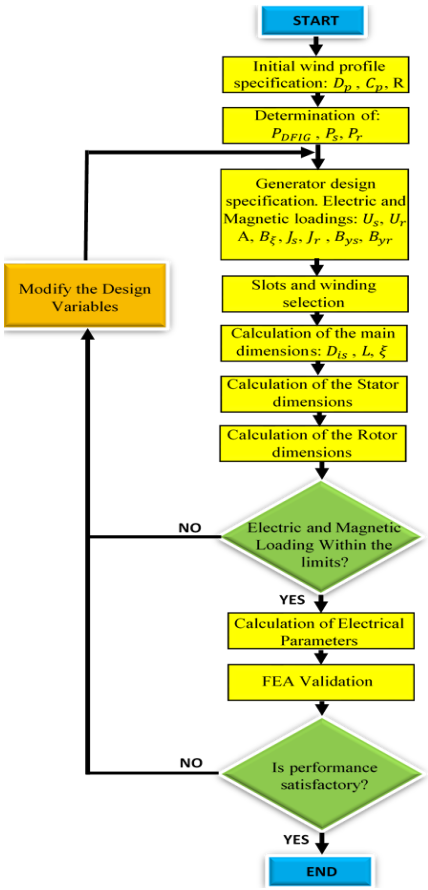

Fig. 2. DFIG sizing flowchart

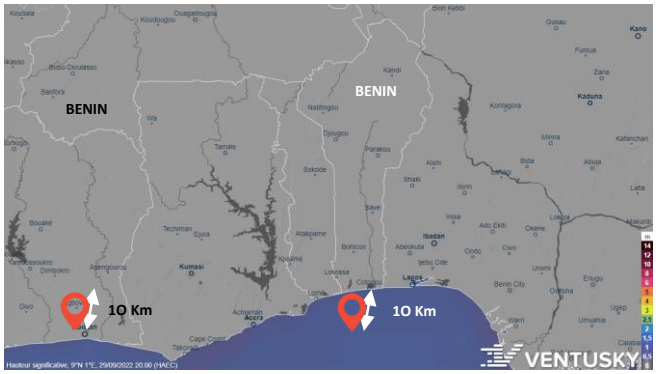

Fig. 3. Coastal zone of Benin [7]

The aerodynamic power (P_{ae}) recoverable by the turbine shaft is given by the relation (2).

$$\mathrm{P_{ae}} = \mathrm{C_p}.\mathrm{P_w} \qquad (2)$$

Where C_p is the power factor.

Assuming that all the aerodynamic power is transmitted to the generator then the power of the generator (P_{DFIG}) is equal to the recoverable aerodynamic power. Hence $P_{DFIG} = P_{ae}$.

For $C_p = 0.44$ and $R = 25m$ we obtain $P_{DFIG} = 690.747\ kW$.

The geometry of the proposed DFIG for sizing is shown in Fig. 4. One can notice that it is composed of a wound slot stator and a wound slot rotor.

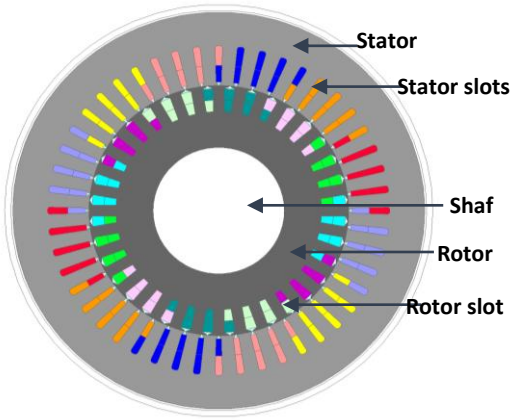

Fig. 4. Geometry of the DFIG

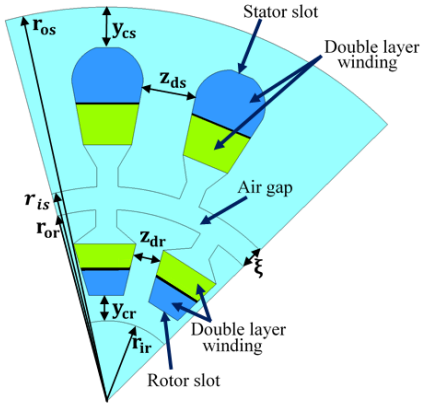

Fig. 5. Cross-section of the DFIG

Table 1. Initial DFIG data

Designation	Symbol	Unite	Value
Power	P_G	kW	690.747
Stator Rated voltage	U_s	V	690
Rotor Rated voltage	U_r	V	690
Frequency	f	Hz	50
Number of pole pair	p	-	2
Rated slip	s	-	0.2
Efficiency	η	-	0.95
Power factor	$\cos\varphi$	-	1
Air gap flux density	B_ξ	T	0.8
Synchronous speed	Ω_s	rpm	1500
Rated speed	Ω_n	rpm	1800
Number of stator slot	Q_s	-	48
Number of rotor slot	Q_r	-	36
Stack length/pole pitch	λ	-	1.3
form factor	k_f	-	1.1
Linear current density	A	kA/m	58.6
Flux density shape factor	α_i	-	0.64
Stator current density	J_s	(A/mm^2)	4.4
Rotor current density	J_r	(A/mm^2)	7
Stator chorded coil windings	ε_s		5/6
Rotor chorded coil windings	ε_r		7/9

Fig. 5 shows a cross-section of the DFIG indicating the geometrical parameters to be determined. The windings used in both the stator and the rotor are double layer.

The first four geometrical parameters to be determined are: the inner radius of the stator (r_{is}), the thickness of the air gap (ξ), the outer radius of the rotor (r_{or}) and the length L of the generator.

The initial DFIG data are shown in Table 1.

The powers of the stator (P_s) and the rotor (P_r) of the generator have the formula [9,10,11]:

$$\mathrm{P_s} = \frac{\mathrm{P_{DFIG}}}{1+\mathrm{s}} \tag{3}$$

$$\mathrm{P_r} = |\mathrm{s}|\mathrm{P_s} \tag{4}$$

For the determination of r_{is} the following relation is used [12]:

$$\mathrm{r_{is}} = \frac{1}{2}\left[\sqrt[3]{\frac{2.\mathrm{p}^2\mathrm{K_E}\mathrm{P_s}}{\eta\lambda \mathrm{f A}.\,\mathrm{k_f}\alpha_\mathrm{i}\pi^3\mathrm{B}_\xi \mathrm{k_{bs}}\cos\varphi}}\right] \tag{5}$$

With:

$$\mathrm{K_E} = 0.98 - .005\mathrm{p} \tag{6}$$

And $k_{bs}$the stator winding factor defined by:

$$\mathrm{k_{bs}} = \sin\left(\varepsilon_\mathrm{s}.\frac{\pi}{2}\right) \times \frac{1}{2\mathrm{q_s}\sin\left(\frac{\pi}{6\mathrm{q_s}}\right)} \tag{7}$$

With q_s the number of slots per pole and per phase of the stator such that:

$$\mathrm{q_s} = \frac{\mathrm{Q_s}}{6\mathrm{p}} \tag{8}$$

In the same way the rotor winding factor k_{br} is defined by:

$$k_{br} = \sin\left(\varepsilon_r.\frac{\pi}{2}\right) \times \frac{1}{2q_r\sin\left(\frac{\pi}{6q_r}\right)} \tag{9}$$

With q_r the number of slots per pole and per phase of the rotor such that:

$$q_r = \frac{Q_r}{6p} \tag{10}$$

The air gap thickness is determined by the following relationship (11):

$$\xi = \left(0.1 + .012\sqrt[3]{\mathrm{P_s}}\right).10^{-3} \tag{11}$$

The outer radius of the rotor can be deduced from equations (5) and (11) by the relation:

$$\mathrm{r_{or}} = \mathrm{r_{is}} - \xi \tag{12}$$

The length of the generator is calculated by the formula:

$$\mathrm{L} = \frac{\lambda\pi\mathrm{r_{is}}}{\mathrm{p}} \tag{13}$$

A. Stator Dimension

At the stator semi-closed rounded slots is chosen. The geometry and geometrical parameters associated with this slot are presented in Fig. 6.

The values of the opening of the slot hysm (z_{s1}), height of the slot hysm (y_{s1}) and height at the upper part of the slot (y_{s2}) are fixed by experiments and are respectively equal to : $z_{s1} = 3\,mm$; $y_{s1} = 1\,mm$; $y_{s2} = 2.5\,mm$.

The following relationships are posed: $z_{s2} = 3.z_{s1}$ and $z_{s3} = 4.z_{s1}$. The section of the stator slot (A_{es}) is calculated by the following equation:

$$\mathrm{A_{es}} = \frac{\pi\mathrm{D_{is}A}}{\mathrm{k_{fi}Q_sJ_s}} \tag{14}$$

With D_{is} the inner diameter of the stator and k_{fi} the stator slot fill factor.

The expression of y_{s4} as a function of A_{es} is established by equation (15).

$$\mathrm{y_{s4}} = \frac{8\mathrm{A_{es}} - \mathrm{z_{s1}^2}(9\pi+12)}{28\mathrm{z_{s1}}} \tag{15}$$

The calculation of y_{s4} allows us to deduce the slot depth y_{s3}, the slot height y_{ecs} and the stator tooth height y_{ds} by the following system of equations:

$$\begin{cases} \mathrm{y_{s3}} = \mathrm{y_{s4}} + \frac{3}{2}\mathrm{z_{s1}} \\ \mathrm{y_{ecs}} = \mathrm{y_{s2}} + \mathrm{y_{s3}} \\ \mathrm{y_{ds}} = \mathrm{y_{ecs}} + \mathrm{y_{1s}} \end{cases} \tag{16}$$

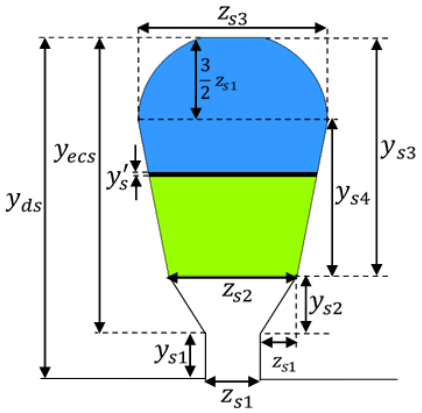

Fig. 6. Stator slot geometry

The width of the tooth (z_{ds}) and the height of the stator yoke (y_{cs}) have the following expressions:

$$z_{ds} = \frac{\pi(D_{is} - 2y_{s1} + 2y_{s2})}{Q_s} - 3z_{s1} \quad (17)$$

$$y_{cs} = \frac{\alpha_i \pi D_{is} B_\xi}{4pB_{ys}} \quad (18)$$

where B_{ys} is the flux density in the stator yoke equal here to 1.5T.

The external radius of the stator is therefore:

$$r_{os} = y_{cs} + r_{is} + y_{ds} \quad (19)$$

B. Rotor Dimension

At the rotor semi-closed slots of trapezoidal shape is chosen. Fig. 7 shows the different parameters of this slot.

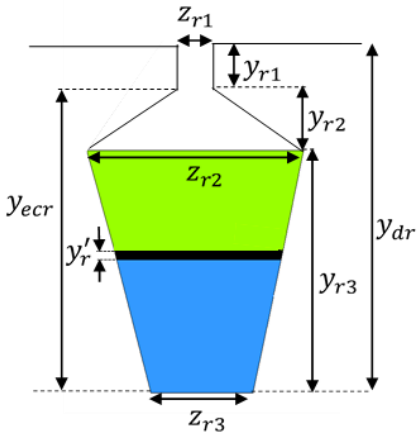

Fig. 7. Stator slot geometry

The opening of the slot hysm, the height of the slot hysm and the height at the upper part of the rotor slot hysm are respectively: $z_{r1} = 2.5\,mm$, $y_{r1} = 1\,mm$ and $y_{r2} = 3\,mm$.

The first things to be determined is the cross-sectional area of the slot (A_{er}) and the width of the rotor tooth (z_{dr}) by the following relationships:

$$A_{er} = \frac{\pi D_{or} A}{k_{fi} Q_r J_r} \quad (20)$$

$$z_{dr} = \frac{\pi D_{or} B_\xi}{Q_r B_{tr}} \quad (21)$$

With D_{or} the external diameter of the rotor and B_{tr} the induction in the rotor teeth equal to 1.6T in our case.

Then, the rotor slot depth y_{r3} is determine by solving the following second-degree equation:

$$\frac{\pi}{Q_r} y_{r3}^2 + \left[z_{dr} - \frac{2\pi(r_{or} - y_{r1} - y_{r2})}{Q_r}\right] y_{r3} + A_{er} = 0 \quad (22)$$

The height of the rotor slot (y_{ecr}) and the height of the rotor tooth (y_{dr}) are calculated by the following system:

$$\begin{cases} y_{ecr} = y_{r2} + y_{r3} \\ y_{dr} = y_{ecr} + y_{r1} \end{cases} \quad (23)$$

The height of the rotor y_{cr} is calculated by equation (24).

$$y_{cr} = \frac{\alpha_i \pi D_{or} B_\xi}{4pB_{yr}} \quad (24)$$

where B_{yr} is the flux density in the rotor yoke equal to 1.4T.

The expressions of the large base z_{r2} and the small base z_{r3} are presented in the system of equation (25).

.

$$\begin{cases} z_{r2} = \frac{2\pi}{Q_r}(r_{or} - y_{r1} - y_{r2}) - z_{dr} \\ z_{r3} = \frac{2\pi}{Q_r}(r_{or} - y_{r1} - y_{r2} - y_{r3}) - z_{dr} \end{cases} \quad (25)$$

The inner radius of the rotor has the formula:

$$r_{ir} = r_{or} - y_{dr} - y_{cr} \quad (26)$$

C. Determination of Electrical Parameters

The maximum ambient operating temperature of the DFIG is set equal to 115°C. The resistances of the stator (R_s) and the rotor (R_r) at this high temperature are calculated by the following equations [12]:

$$\mathrm{R_s} = \frac{2\rho_{\mathrm{co}_{115}\circ}\mathrm{N_s}\left(\mathrm{L} + \mathrm{L_{end\_s}}\right)}{\mathrm{A_{co\_s}}} \tag{27}$$

$$R_r = \frac{2\rho_{co_{115}\circ}N_r\left(L + L_{end\_r}\right)}{A_{co\_r}} \tag{28}$$

where $\rho_{co_{115}\circ}$ is the copper resistivity at 115°, N_s and N_r are the number of turns per phase at the stator and rotor respectively, L_{end_s} and L_{end_r} are the end connection length at the stator and rotor respectively, A_{co_s} and A_{co_r} are the conductor cross section at the stator and rotor respectively. A_{co_s} and A_{co_s} are defined by:

$$\mathrm{A_{co\_s}} = \frac{\mathrm{I_{sn}}}{\mathrm{a_1 J_s}} \tag{29}$$

$$\mathrm{A_{co\_r}} = \frac{\mathrm{I_{rn}}}{\mathrm{a_1 J_r}} \tag{30}$$

Where I_{sn} and I_{rn} are respectively the RMS currents at the stator and at the rotor defined by the equation system (31) and a_1 is the number of current paths in parallel equal here to 1.

$$\begin{cases} \mathrm{I_{sn}} = \dfrac{\mathrm{P_s}}{\sqrt{3}\mathrm{U_s}\eta\cos\varphi} \\ \mathrm{I_{rn}} = \mathrm{s}\dfrac{\mathrm{U_s}}{\mathrm{U_r}}\mathrm{I_{sn}} \end{cases} \tag{31}$$

L_{end_s} and L_{end_r} are calculated by the relations (32) and (33) for a machine with 2 pairs of poles:

$$\mathrm{L_{end\_s}} = 2\mathrm{y_1} - 0.02 \tag{32}$$

$$\mathrm{L_{end\_r}} = 2\mathrm{y_2} - 0.02 \tag{33}$$

With y_1 and y_2 the coil span respectively at the stator and rotor defined by:

$$\mathrm{y_1} = \varepsilon_\mathrm{s}\frac{\pi\mathrm{D_{is}}}{2\mathrm{p}} \tag{34}$$

$$\mathrm{y_2} = \varepsilon_\mathrm{r}\frac{\pi\mathrm{D_{or}}}{2\mathrm{p}} \tag{35}$$

For the calculation of the stator and rotor leakage inductances, we use equations (36) and (37) [13].

$$\mathrm{L_s} = \frac{12\mu_0\mathrm{LN_s^2}}{\mathrm{Q_s}}\lambda_\mathrm{s} \tag{36}$$

$$\mathrm{L_r} = \frac{12\mu_0\mathrm{LN_r^2}}{\mathrm{Q_r}}\lambda_\mathrm{r} \tag{37}$$

With μ_0 the relative vacuum permeability, λ_s and λ_r the respective stator and rotor slots leakage geometrical permeance defined by the relations:

$$\lambda_s = k_{1s}\frac{y_{s4} - y_s^{'}}{3z_{s2}} + k_{2s}\left(\frac{y_s^{'}}{z_{s2}} + \frac{y_{s1}}{z_{s1}} + \frac{y_{s2}}{z_{s2} - z_{s1}}ln\left(\frac{z_{s2}}{z_{s1}}\right)\right) + \frac{y_s^{'}}{4z_{s2}} \tag{38}$$

$$\lambda_r = k_{1r}\frac{y_{r3} - y_r^{'}}{3z_{r2}} + k_{2r}\left(\frac{y_r^{'}}{z_{r2}} + \frac{y_{r1}}{z_{r1}} + \frac{y_{r2}}{z_{r2} - z_{r1}}ln\left(\frac{z_{r2}}{z_{r1}}\right)\right) + \frac{y_r^{'}}{4z_{r2}} \tag{39}$$

Where the constants k_{1s}, k_{2s}, k_{1r} and k_{2r} have the expression:

$$\begin{cases} \mathrm{k_{1s}} = 1 - \left(\dfrac{9}{16}\right)\varepsilon_1 \\ \mathrm{k_{2s}} = 1 - \left(\dfrac{3}{4}\right)\varepsilon_1 \\ \mathrm{k_{1r}} = 1 - \left(\dfrac{9}{16}\right)\varepsilon_2 \\ \mathrm{k_{2r}} = 1 - \left(\dfrac{3}{4}\right)\varepsilon_2 \end{cases} \tag{40}$$

With:

$$\begin{cases} \varepsilon_1 = 1 - \varepsilon_\mathrm{s} \\ \varepsilon_2 = 1 - \varepsilon_\mathrm{r} \end{cases} \tag{41}$$

The parameters of the DFIG obtained after sizing are shown in Table 2.

D. DFIG Simulation by FEA

The flux 2D, 2022 version software has been used to simulate the sized DFIG. For that rotor turn is fixed at the nominal speed of 1800 rpm. This corresponds to an operation in supersynchronous mode. The flux density map and the flux lines of the DFIG obtained are shown in figures 8 and 9 respectively.

The Fig. 10 shows the superposition of the radial and tangential flux densities obtained at the center of the DFIG air gap. It can be noticed that the flux density in the air gap is mainly radial and that it' s not perfectly sinusoidal. This is due to the type of winding used in the rotor.

Table 2. The DFIG parameters obtained

	Symbol	Value
Power	$P_s\ (kW)$	575.6225
	$P_r\ (kW)$	115.1245
	$P_{DFIG}\ (kW)$	
Geometric parameters	$r_{is}(mm)$	212.2
	$r_{ir}(mm)$	107.25
	$\xi(mm)$	1.1
	$r_{os}(mm)$	336.8
	$r_{or}(mm)$	211.1
	$L(mm)$	433.3
	$y_{ds}(mm)$	67.7
	$y_{dr}(mm)$	43.2
	$\mathrm{y_{cs}}(mm)$	56.9
	$\mathrm{y_{cr}}(mm)$	60.6
	$\mathrm{z_{ds}}(mm)$	19
	$\mathrm{z_{dr}}(mm)$	18.4
Electrical parameters	$R_s(\Omega)$	0.0115
	$R_r(\Omega)$	0.0876
	$L_s(mH)$	0.304
	$L_r(mH)$	0.185

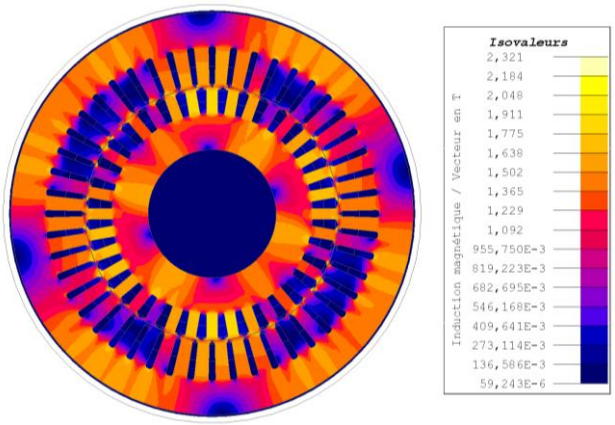

Fig. 8. DFIG flux density map

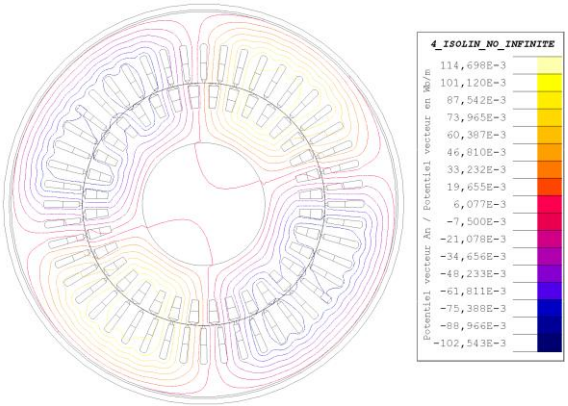

Fig. 9. DFIG flux lines map

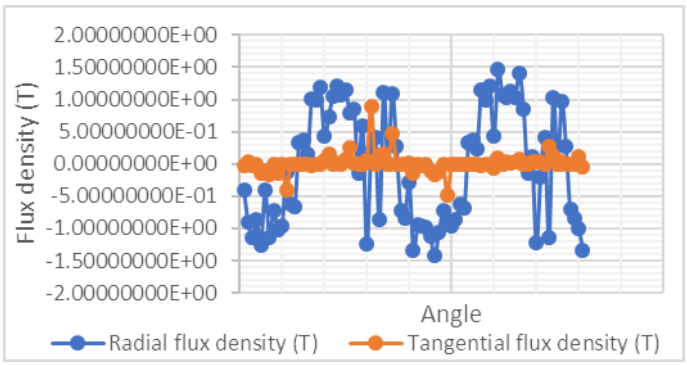

Fig. 10. Radial and tangential flux densities curves in the air gap

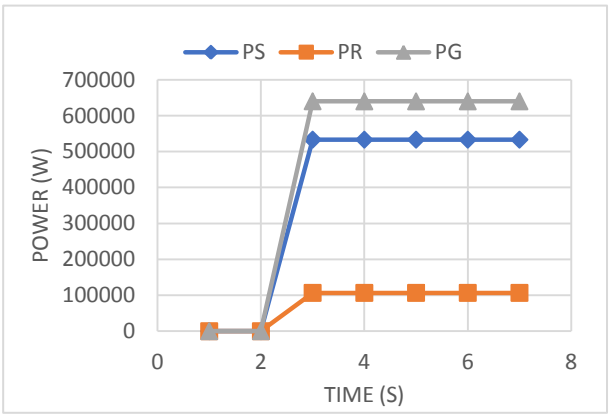

Fig. 11. DFIG powers curves

In the same way the curve of the powers developed by the DFIG in this mode of operation is shown in Fig. 11.

It can be seen that the DFIG takes at most 3s before reaching its steady state. The maximum powers at the stator and rotor are respectively 533.3 kW and 106.66 kW. A maximum power of 640 kW is reached and is developed by the generator. This power value is close to the theoretical power of the generator. this shows that the values of the parameters found during the sizing are acceptable.

4. DFIG THERMAL MODEL

To establish the thermal model, it is important to determine the different losses in the generator. These losses are dissipated in the form of heat and are classified into two categories: joule losses and iron losses. The respective stator and rotor losses P_{js} and P_{jr} are calculated analytically by formulas (42) and (43). As for the respective iron losses P_{fs} and P_{fr} at the stator and rotor, they are determined by the FEA.

$$\mathrm{P_{js}} = 3\mathrm{R_s}\mathrm{I_{sn}^2} \tag{42}$$

$$\mathrm{P_{jr}} = 3\mathrm{R_r}\mathrm{I_{rn}^2} \tag{43}$$

The values of the different losses are shown in Table 3.

Table 3. Loss values at the DFIG level

Losses	Values
$P_{fs}\ (kW)$	1.493
$P_{fr}\ (kW)$	0.391
$P_{js}\ (kW)$	8.868
$P_{jr}\ (kW)$	2.702

The results of the calculation of the heat sources are obtained by dividing the losses by the total volumes corresponding to each DFIG domain. Table 4 below summarizes the heat sources obtained.

Table 4. Heat source in each domain

Domain	Losses (kW)	Volume (m^3)	Heat source (W/m^3)
Stator winding	8.868	0.013543	$6.55\ 10^5$
Rotor winding	2.702	0.008738	$3.09\ 10^5$
Stator yoke	1.493	0.079072	$1.89\ 10^4$
Rotor yoke	0.391	0.036002	$1.09\ 10^4$

Thanks to these data the simulation of the DFIG is done in thermal steady state under flux 2D, 2022 version software. The temperature map of the DFIG is shown in Fig. 12. On this map, it can be notice that the temperature of the DFIG varies from 25°C to 92.94°C. This range of temperature variation is satisfactory since the maximum value of the temperature that the generator can support (115°C) is not reached. This result shows that the generator sized does not heat up excessively in nominal operation.

Fig. 13-a shows on the one hand a half view of the temperature variations observed at the level of the rotor and stator yokes and on the other hand Fig. 13-b shows a half view of the temperature variations inside the rotor and stator slots.

It can be seen that the temperatures in the stator yoke are higher than in the rotor yoke. Similarly, the temperatures in the stator slots are higher than in the rotor slots. This result is normal because the stator windings carry much higher currents than the rotor windings and generate more Joule losses and therefore more heating. The average temperature obtained in the air gap is 67.09°C.

The minimum and maximum temperature values in each domain of the DFIG are shown in Table 5.

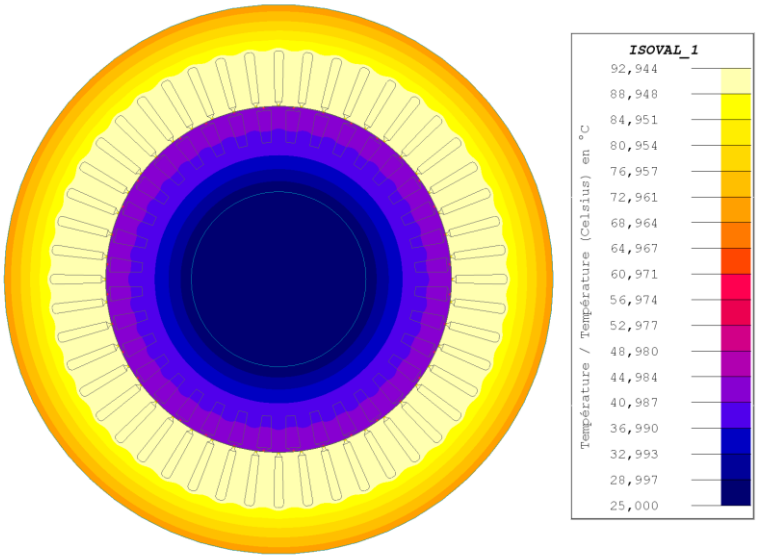

Fig. 12. Temperature map of the DFIG

Table 5. Temperature variation in each domain

Domain	Minimum value	Maximum value
Stator winding	$90.6°C$	$92.94°C$
Rotor winding	$40.51°C$	$41.24°C$
Stator yoke	$70°C$	$92.94°C$
Rotor yoke	$25°C$	$41.43°C$
Air gap	$41.3°C$	$92.87°C$

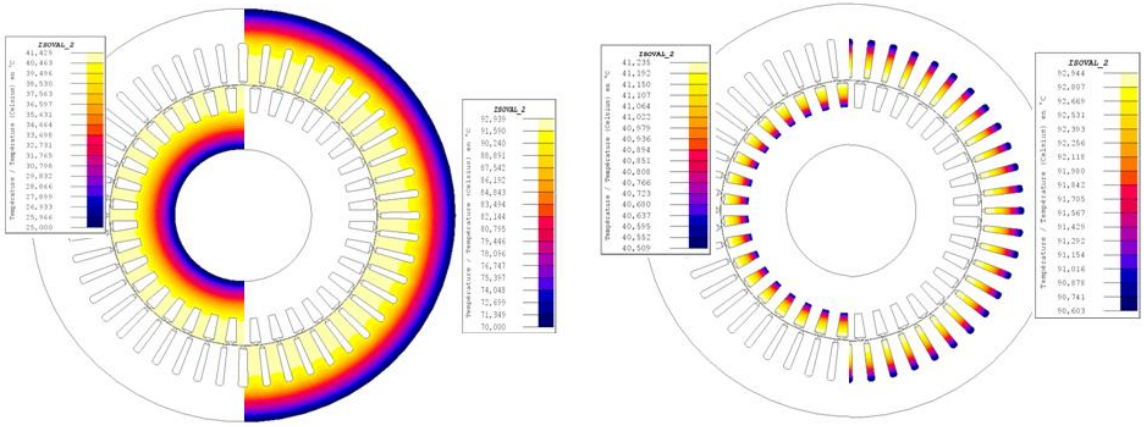

(a) **(b)**

Fig. 13. Half view of the temperature variations. (a) In rotor and stator yokes. (b) Inside the rotor and stator slots

5. CONCLUSION

In this paper the sizing and simulation of the DFIG adapted to the Benin offshore wind profile is presented. For the sizing, we started from an analytical model to obtain the electrical, magnetic and geometrical parameters of the generator. This latter is simulated according to the dynamic and thermal models. The results obtained according to these two models are satisfactory. But only an experimental study of the proposed generator will allow to approve these results. Among other things, this paper can be used as a guide for the constructors within the framework of the design of the DFIG.

COMPETING INTERESTS

Authors have declared that no competing interests exist.

REFERENCES

1. Renewable Energy Market Analysis: Africa and its Regions; 318.
2. The Renewable Energy Transition in Africa, /publications/2021/March/The-Renewable-Energy-Transition-in-Africa. https://www.irena.org/publications/2021/March/The-Renewable-Energy-Transition-in-Africa (consulté le 1 octobre 2022).
3. Gnandji MR, Fifatin FX, Dubas F, Espanet C, et A. Vianou, Etude du Potentiel Energétique Eolien Offshore du Bénin, in Colloque International Francophone portant sur l'Energétique et la Mécanique, Cotonou, Benin, avr. 2018. Consulté le: 1 octobre 2022. [En ligne]. Disponible sur.

   Available:https://hal.archives-ouvertes.fr/hal-02130123
4. Hiremath R, et T. Moger, Comparison of LVRT Enhancement for DFIG-Based Wind Turbine Generator with Rotor-Side Control Strategy, in 2020 International Conference on Electrical and Electronics Engineering (ICE3), Gorakhpur, India, févr. 2020; 216- 220.

   DOI: 10.1109/ICE348803.2020.9122830
5. Rached B, Bensaid M, Elharoussi M, Abdelmounim E. DSP in the loop Implementation of the Control of a DFIG Used in Wind Power System, in 2020 1st International Conference on Innovative Research in Applied Science, Engineering and Technology (IRASET), Meknes, Morocco, avr. 2020;1-6.

   DOI:10.1109/IRASET48871.2020.9092165
6. Prieto Cerón CE, Normandia Lourenço LF, Solís-Chaves JS, Sguarezi Filho AJ. A generalized predictive controller for a wind turbine providing frequency support for a microgrid, energies. 2022;15(7):Art no 7.

   DOI: 10.3390/en15072562
7. Ventusky. Cartes de Prévision Météo.

   Available:https://www.ventusky.com (consulté le 1 octobre 2022).
8. Phan DC, et S. Yamamoto, maximum energy output of a DFIG wind turbine using an improved MPPT-curve method, energies. 2015;8(10):oct:Art no 10.

   DOI: 10.3390/en81011718

9. Ulu C, Kömürgöz G. Electrical design and testing of a 500 kW doubly fed induction generator for wind power applications. Turk J Elec Eng & Comp Sci. 2017; 25:1278-90.
DOI: 10.3906/elk-1512-28

10. Izanlo A, Abdollahi SE, Gholamian SA. A new method for design and optimization of DFIG for wind power applications. Electr Power Compon Syst. Sep 2020;48(14-15):1523-36.
DOI: 10.1080/15325008.2020.1856231

11. OI. Olubamiwa et N. Gule, Performance investigation of DFIG topologies with different design parameters, in 2017 IEEE AFRICON, Cape Town, Sep 2017;1242-7.
DOI: 10.1109/AFRCON.2017.8095660

12. Boldea I, Nasar SA. The induction machines design handbook. 2nd ed; 2010.

13. Pyrhonen J, Jokinen T, Hrabovcová V. Design of rotating electrical machines. Chichester. Sussex, United Kingdom: West; Hoboken, NJ: Wiley; 2008.

Peer-review history:
The peer review history for this paper can be accessed here:
https://www.sdiarticle5.com/review-history/93484